

Supplementary Information

***In situ* exsolved FeNi₃ nanoparticles on nickel doped Sr₂Fe_{1.5}Mo_{0.5}O_{6-δ} perovskite for efficient electrochemical CO₂ reduction reaction**

Houfu Lv,^{a, b, c, ‡} Le Lin,^{a, b, d, ‡} Xiaomin Zhang,^{a, c} Dunfeng Gao,^{a, c} Yuefeng Song,^{a, b, c} Yingjie Zhou,^{a, c} Qingxue Liu,^{a, b, c} Guoxiong Wang^{a, c*} and Xinhe Bao^{a, c*}

^a State Key Laboratory of Catalysis, CAS Center for Excellence in Nanoscience, Dalian Institute of Chemical Physics, Chinese Academy of Sciences, Dalian, 116023, China

^b University of Chinese Academy of Sciences, Beijing, 100039, China

^c Dalian National Laboratory for Clean Energy, Dalian Institute of Chemical Physics, Chinese Academy of Sciences, Dalian, 116023, China

^d School of Physical Science and Technology, ShanghaiTech University, Shanghai, 201210, China

[‡] These authors have contributed equally to this work.

*Email: wanggx@dicp.ac.cn, xhbao@dicp.ac.cn.

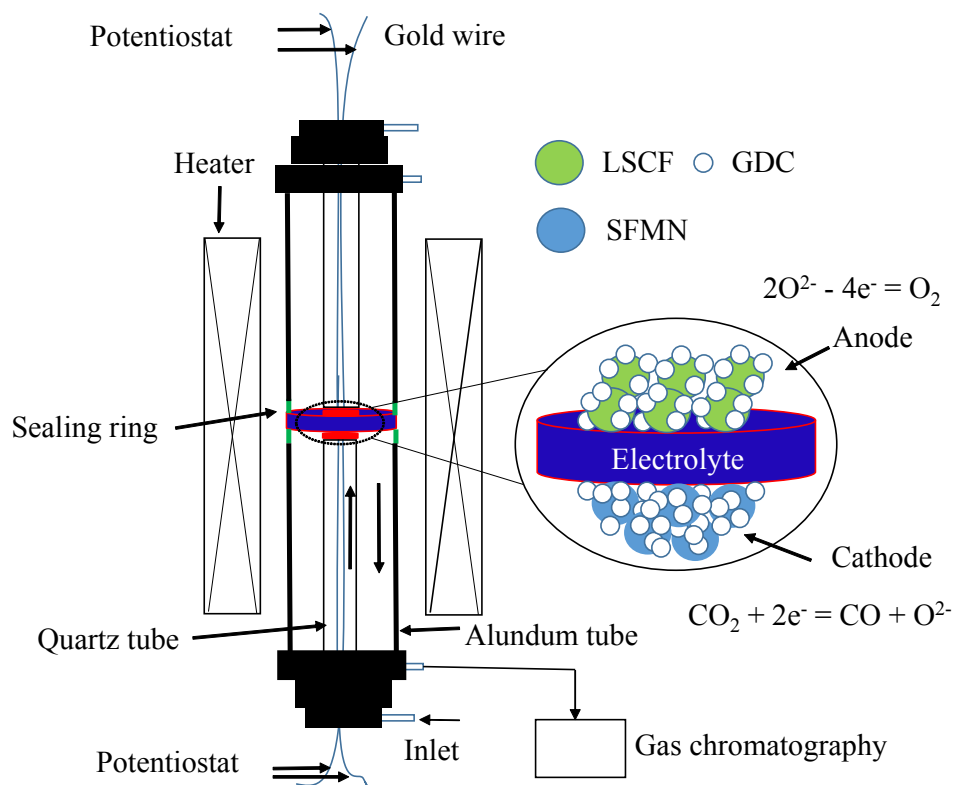


Figure S1. Schematic diagram of the SOEC testing device.

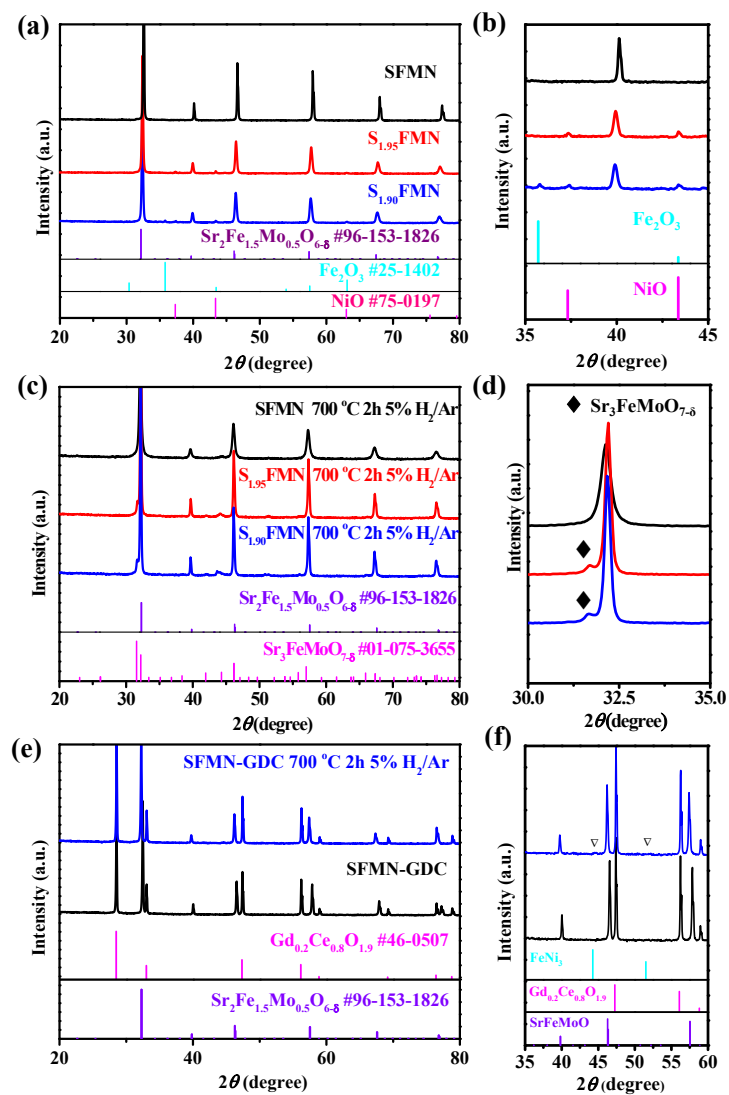


Figure S2. (a) XRD patterns of SFMN, $S_{1.95}$ FMN and $S_{1.90}$ FMN. (b) The enlarged XRD patterns of 35-45° of (a). (c) XRD patterns of SFMN, $S_{1.95}$ FMN and $S_{1.90}$ FMN after reduction treatment in 5 % H_2/Ar at 700 °C for 2 h. (d) The enlarged XRD patterns at 35-45° of (c). (e) XRD patterns of SFMN-GDC and SFMN-GDC after reduction treatment in 5 % H_2/Ar at 700 °C for 2 h. (f) The enlarged XRD patterns at 35-60° of (e)

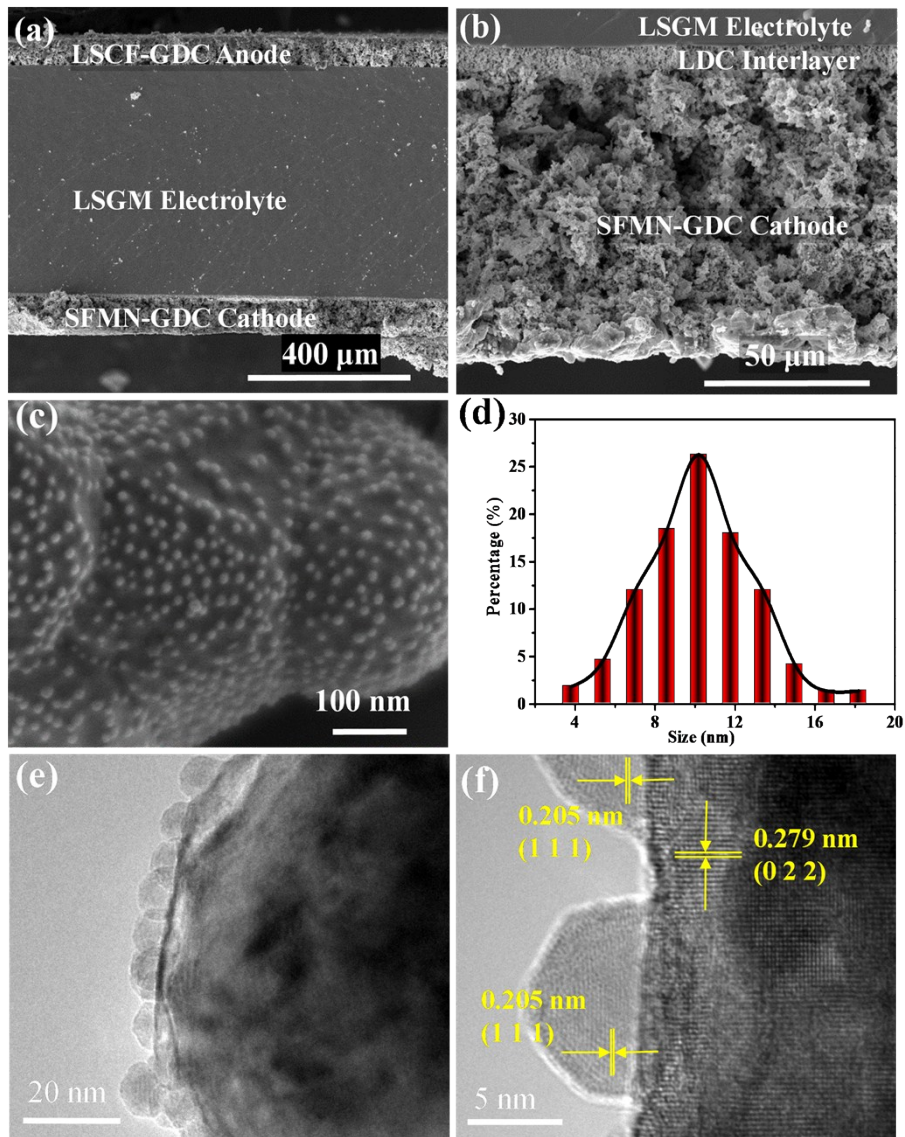


Figure S3. (a) Cross-sectional SEM images of the SFMN-GDC|LDC|LSGM|LSCF-GDC. (b) LSGM|LDC supported SFMN-GDC cathode. (c) SEM image of the FeNi₃@SFMN. (d) Size distribution of FeNi₃ nanoparticles in FeNi₃@SFMN. (e) High-resolution TEM image of FeNi₃@SFMN. (f) The corresponding crystal lattice of FeNi₃ nanoparticles and the perovskite substrate.

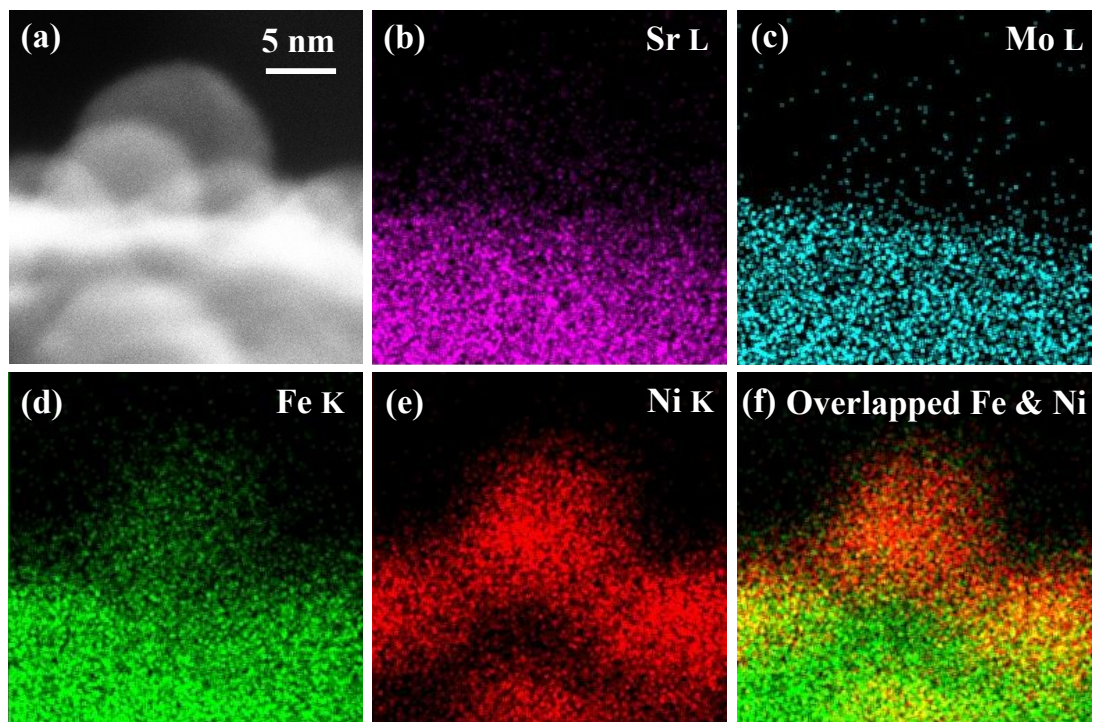


Figure S4. STEM image and element maps of FeNi₃@SFMN. (a) STEM image, (b) Sr maps, (c) Mo maps, (d) Fe maps, (e) Ni maps and (f) overlapped Fe and Ni maps.

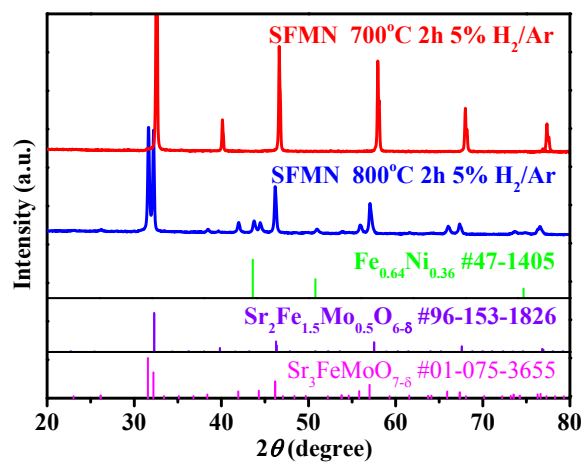


Figure S5. XRD patterns of SFMN after reduction treatment in 5 % H₂/Ar for 2 h at 700 °C and 800 °C.

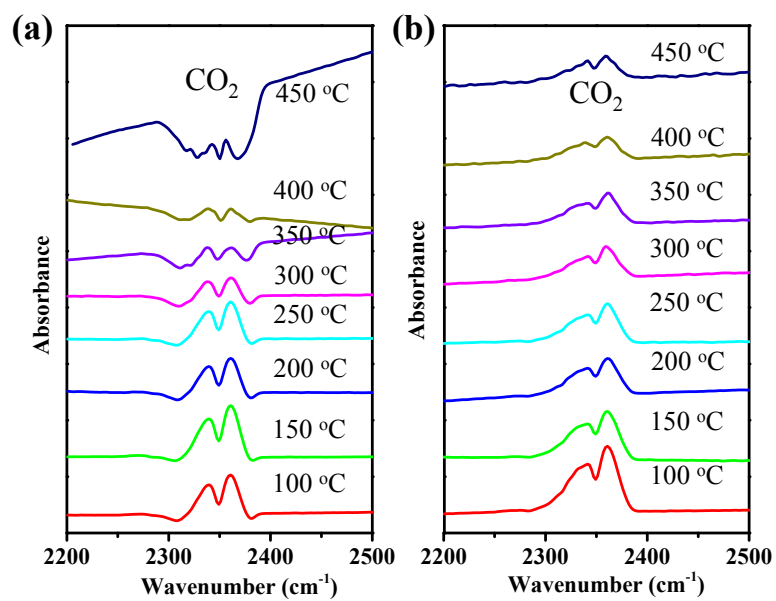


Figure S6. *Quasi in situ* FTIR spectroscopy of CO₂ adsorbed on SFMN (a) and FeNi₃@SFMN (b) from 100-450 °C.

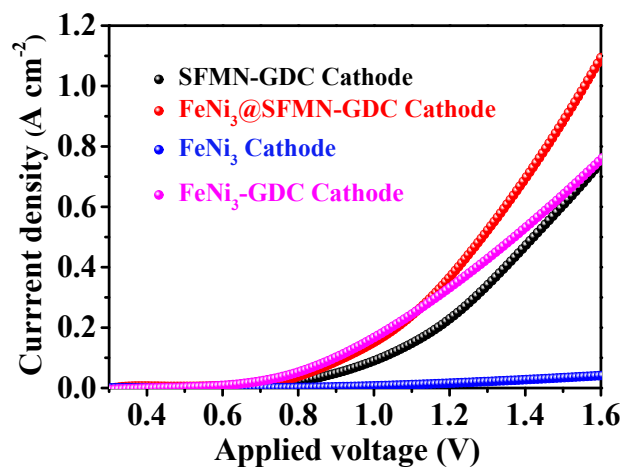


Figure S7. I-V curves of SOECs with SFMN-GDC, FeNi₃@SFMN-GDC, FeNi₃ and FeNi₃-GDC cathodes at 800 °C.

As for the individual FeNi₃ nanoparticles for CO₂RR, we have tested the pure FeNi₃ and FeNi₃-GDC (The mass ratio between Ni and GDC are the same for FeNi₃-GDC and SFMN-GDC cathodes) as the cathodes at the same preparation and test conditions.

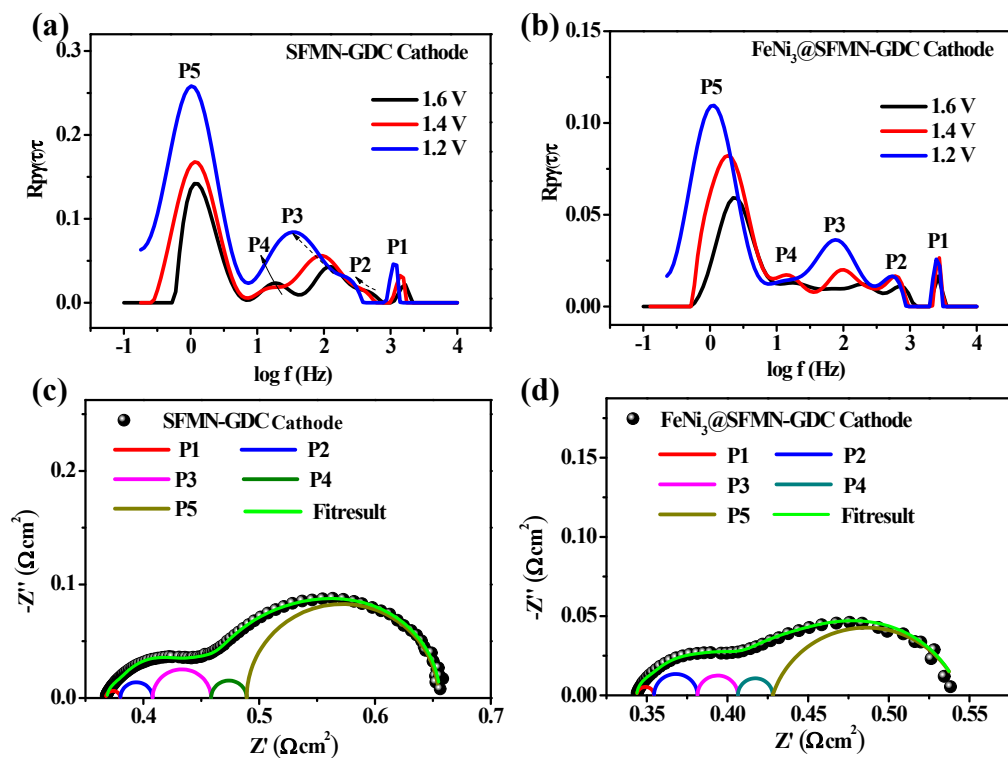


Figure S8. DRT plots of SOECs with SFMN-GDC (a) and FeNi₃@SFMN-GDC cathodes (b) at various voltages and 800 °C. The resolved EIS results of SOECs with SFMN-GDC (c) and FeNi₃@SFMN-GDC (d) cathodes at 1.6 V and 800 °C.

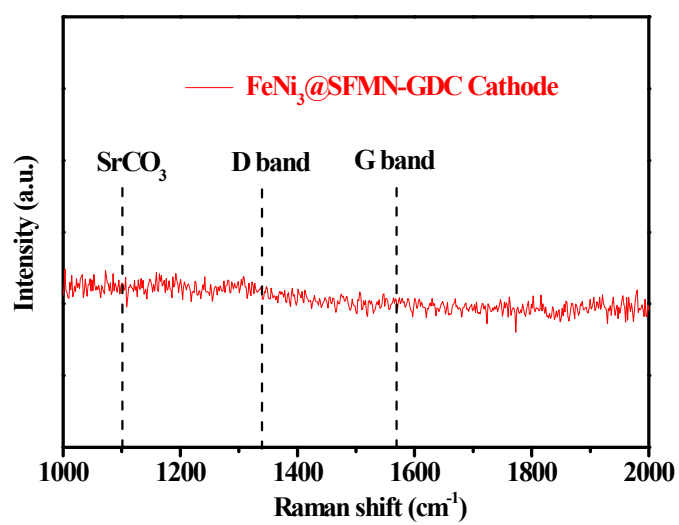


Figure S9 Raman spectra of SOEC with FeNi₃@SFMN-GDC cathode after the stability test.

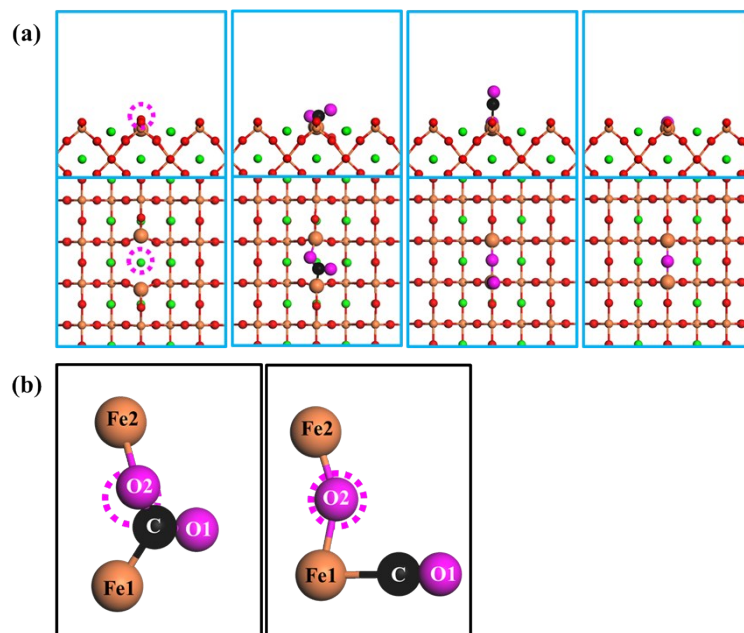


Figure S10. DFT calculation results. (a) Optimized geometry structures of the CO₂RR to CO process over the SFO surface. (b) The local enlarged configurations of CO₂* and CO* over the SFO model.

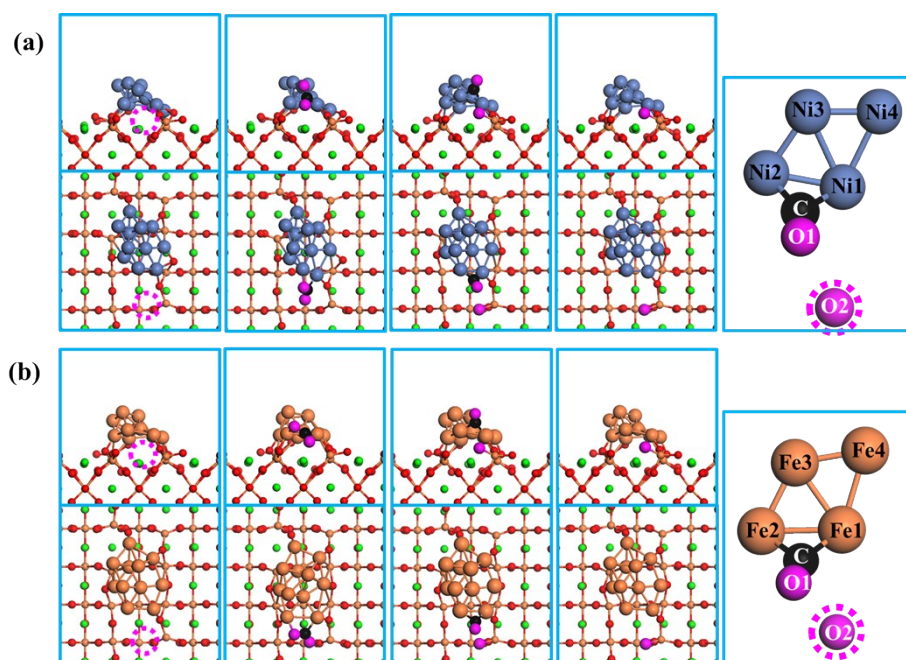


Figure S11. DFT calculation results. Optimized geometry structures of the CO₂RR to CO process including amplified CO* intermediates (right panels) over two kinds of boundary interfaces (a) Ni@SFO and (b) Fe@SFO.

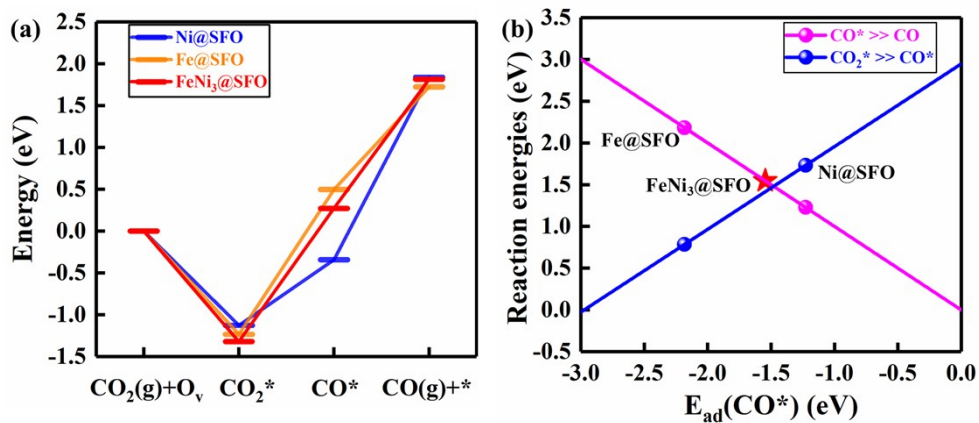


Figure S12. DFT calculation results. (a) Potential energy diagram of the CO_2RR to CO process over different boundary interfaces. * represents surface adsorption site and O_v denotes the surface with oxygen vacancy. (b) Fitted CO^* desorption (CO^* to CO) and CO_2^* activation (CO_2 to CO^*) trends over all three clusters.

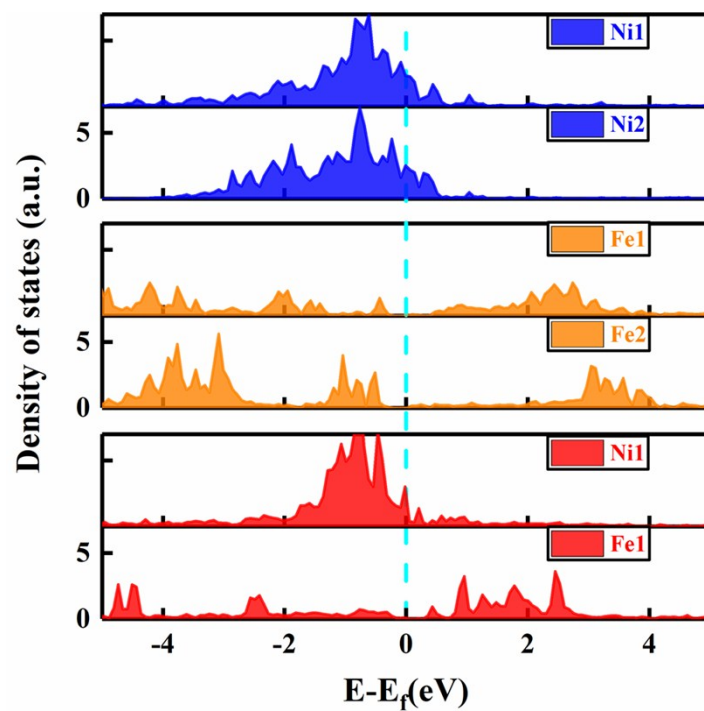


Figure S13. DFT calculation results. The d-projected DOS of active Ni or Fe at the interfaces of Ni@SFO, Fe@SFO and FeNi₃@SFO.

Table S1. The stability and formation energies of oxygen vacancy of SMO (0 2 2) plane.

N_{Ov}	E_{vac}/eV	E_{pri}/eV	E_{ov}/eV
1	-291.75	-300.42	1.20

Firstly, we explored a stable O-terminated SMO (0 2 2) surface in the same method with SFO (0 2 2) models. Next, the formation energies of oxygen vacancy is calculated by the formula: $E_{Ov} = E_{vac} + E_{H_2O} - E_{pri} - E_{H_2}$, where E_{H_2O} and E_{H_2} are the energies of H₂O and H₂ in gas phase, respectively.. Therefore, we deduce that Mo atom is easily bonded to oxygen atoms because the formation energies of oxygen vacancy is that high through hydrogen reduction.

Table S2. Comparison of the stability of two kinds of termination planes for SFO (0 2 2) plane.

<i>unit</i>	<i>Stoichiometry</i>			E_t	A	γ
	<i>Sr</i>	<i>Fe</i>	<i>O</i>	<i>eV</i>	\AA^2	$eV/\text{\AA}^2$
bulk	1	1	3	-32.93	N/A	N/A
(0 2 2)-1	3	3	9	-93.78	21.08	0.24
(0 2 2)-2				-92.84		0.28

Here, (1) *Stoichiometry* gives the ratio of Sr, Fe and O atoms in supercell. (2) E_t is the total energy from DFT calculations. (3) A is the surface area calculated by a×b (a and b refer to the lattice parameters). (4) γ is the surface energy, which obtained by the formula : $\gamma = \frac{1}{A}(E_{surf} - NE_{bulk})$, where N is the number of Fe in (0 2 2) plane models. And the smaller the γ value, the more stable the model.

Table S3. The formation energies of oxygen vacancy for different models.

	N_{Ov}	E_{vac}/eV	E_{pri}/eV	E_{ov}/eV
SFO	1	-722.90	-729.92	-0.45
Ni@SFO	1	-772.50	-778.86	-1.11
Fe@SFO	1	-776.40	-781.23	-1.00
FeNi ₃ @SFO	1	-774.29	-780.67	-1.09

Here, (1) N_{Ov} is the number of oxygen vacancies in supercell. (2) E_{vac} is the total energy of the oxygen-defected models. (3) E_{pri} is the total energy of the pristine models referred to the oxygen-defected models. (4) E_{ov} is the formation energies of oxygen vacancy, which were calculated as $E_{Ov} = E_{vac} + E_{H_2O} - E_{pri} - E_{H_2}$, where E_{H_2O} and E_{H_2} are the energies of H₂O and H₂ in gas phase, respectively.

Table S4. XPS analysis of Ni 2*p* for SFMN and FeNi₃@SFMN samples.

Sample	B.E. Ni 2 <i>p</i> _{3/2} (eV)		Ni ⁰ (at.%)	Ni ²⁺ (at.%)
	Ni ⁰	Ni ²⁺		
SFMN		854.4/855.9	0	100
FeNi ₃ @SFMN	852.5/857.8	854.5/856.0	47.97	52.03

Table S5. XPS analysis of Fe 2*p* for SFMN and FeNi₃@SFMN samples.

Sample	B.E. Fe 2 <i>p</i> _{3/2} (eV)			Fe ⁰ (at.%)	Fe ²⁺ (at.%)	Fe ³⁺ (at.%)
	Fe ⁰	Fe ²⁺	Fe ³⁺			
SFMN	709.6	711.4		0	50.13	49.87
FeNi ₃ @SFMN	704.5	710.2	711.7	3.30	58.98	37.72

Table S6. XPS analysis of Mo 3d for SFMN and FeNi₃@SFMN samples.

Sample	B.E. Mo 3d _{5/2} (eV)		Mo ⁵⁺ (at.%)	Mo ⁶⁺ (at.%)
	Mo ⁵⁺	Mo ⁶⁺		
SFMN		232.0/235.1	0	100
FeNi ₃ @SFMN	231.7/234.7	232.8/235.9	6.45	93.55

Table S7. XPS analysis of O 1s for SFMN and FeNi₃@SFMN samples.

Sample	B.E. O 1s (eV)		O _{lat.} (at.%)	O _{ads.} (at.%)
	O _{lat.}	O _{ads.}		
SFMN	528.7	530.9/532.1	42.31	57.69
FeNi ₃ @SFMN	529.5	531.0/532.2	44.21	55.79

Table S8. The models of SFO (0 2 2) surface and interface.

<i>unit</i>	<i>Stoichiometry</i>				<i>E_t</i> <i>eV</i>
	<i>Sr</i>	<i>Fe</i>	<i>O</i>	<i>Ni</i>	
SFO	24	24	72	N/A	-729.92
Ni@SFO	24	24	72	11	-778.86
Fe@SFO	24	35	72	N/A	-782.88
FeNi ₃ @SFO	24	26	72	9	-780.67